





Wastewater-influenced estuaries are characterized by disproportionately high nitrous oxide emissions but overestimated IPCC emission factor

Yue Dong ^{1,2}, Jia Liu^{3,4}, Xiang Cheng^{1,2,5}, Fuqiang Fan^{1,2}, Wei Lin^{1,2}, Chunyang Zhou^{1,2}, Shengrui Wang ^{1,2,5}✉, Shangbin Xiao ^{3,4}✉, Chenghao Wang ^{6,7}✉, Yu Li^{1,2} & Changlin Li^{1,2}

Estuaries play an important role in the global nitrous oxide budget. However, considerable uncertainties exist in estimating their nitrous oxide emissions, largely due to anthropogenic impacts, particularly wastewater discharge. Here we investigate nitrous oxide emission dynamics in the Pearl River Estuary through advanced high-resolution, real-time measurements. Results suggest that Pearl River Estuary is a strong nitrous oxide emission source (1.05 Gg yr⁻¹; range: 0.92–1.23 Gg yr⁻¹) with pronounced spatial heterogeneity. Wastewater discharge substantially impacts emissions by introducing abundant nutrients, altering carbon-to-nitrogen stoichiometry, and stimulating biochemical processes. A meta-analysis further reveals the widespread enhancement of nitrous oxide emission induced by wastewater nitrogen input in global estuaries, with nitrous oxide emission factors considerably lower than that suggested by the IPCC owing to progressive biological saturation. Consequently, refining emission factor estimates through comprehensive bottom-up studies is imperative to improve the understanding of estuarine contributions to the global nitrous oxide budget.

¹Guangdong-Hong Kong Joint Laboratory for Water Security, Beijing Normal University, 519087 Zhuhai, China. ²Center for Water Research, Advanced Institute of Natural Sciences, Beijing Normal University, 519087 Zhuhai, China. ³College of Hydraulic and Environment Engineering, China Three Gorges University, 443002 Yichang, China. ⁴Hubei Field Observation and Scientific Research Stations for Water Ecosystem in Three Gorges Reservoir, China Three Gorges University, 443002 Yichang, China. ⁵College of Water Sciences, Beijing Normal University, 100875 Beijing, China. ⁶School of Meteorology, University of Oklahoma, Norman, OK 73072, USA. ⁷Department of Geography and Environmental Sustainability, University of Oklahoma, Norman, OK 73019, USA. ✉email: wangsr@bnu.edu.cn; shangbinx@163.com; chenghao.wang@ou.edu

Nitrous oxide (N_2O) is a primary stratospheric ozone-depleting substance and the third most important long-lived greenhouse gas (GHG)¹, with a global warming potential 273 times that of CO_2 over a 100-year horizon². As an important source of N_2O emissions to the atmosphere³, estuaries account for approximately 33% of the global oceanic N_2O emissions, despite covering only 0.4% of the world's ocean area⁴. However, N_2O emissions from estuaries remain a poorly constrained component in the global N_2O budget³. Many densely populated estuaries receive a substantial amount of wastewater discharged from surrounding urban areas⁵. The wastewater input, together with dynamic anthropogenic–estuarine interactions, leads to strong spatial variations and great uncertainties in estuarine N_2O emissions^{5,6}. Accurately characterizing their spatial heterogeneity requires high-resolution monitoring, which is critical to improving our understanding of regional and global N_2O budgets.

Estuarine N_2O is primarily produced through biochemical processes, including nitrification, denitrification, nitrifier denitrification, and dissimilatory nitrate reduction to ammonium (DNRA)⁷. The production of estuarine N_2O is governed by nutrients, organic carbon, dissolved oxygen, microbial activity, coastal vegetation, and hydrologic conditions^{8–11}. In particular, anthropogenic sources, especially wastewater discharge, are critical contributors to estuarine nutrient input¹², accounting for an estimated ~50% of the total nitrogen load in estuarine and riverine watersheds worldwide^{13,14}. Discharges from wastewater treatment plants are typically characterized by low carbon-to-nitrogen ratios¹⁵ and low chemical oxygen demand to total nitrogen ratios¹⁶. These conditions stimulate denitrification activity due to the abundant $\text{NO}_3\text{-N}$ load, resulting in a high $\text{N}_2\text{O}:\text{N}_2$ ratio with limited availability of dissolved organic carbon (DOC) (as electron donor) relative to $\text{NO}_3\text{-N}$ (as electron acceptor)^{17–19}.

To estimate estuarine N_2O emissions, the Intergovernmental Panel on Climate Change (IPCC) employs dissolved nitrate and the emission factor (EF_{5e}), assuming a linear relationship between $\text{N}_2\text{O-N}$ and $\text{NO}_3\text{-N}$ ²⁰. However, previous studies have suggested substantial uncertainties in the estimated global estuarine emissions when using the current IPCC EF_{5e} ^{13,21,22}. Considering that the factors affecting N_2O emissions in natural estuaries differ from those influenced by anthropogenic activities^{23,24}, the use of a universal EF_{5e} for all estuaries worldwide is questionable^{13,25}. Furthermore, the response pattern of N_2O to N load could differ when there is high nutrient input with altered C:N stoichiometry in wastewater-influenced estuaries^{13,19}. Especially, it remains unclear whether a further increase in N input would linearly translate to elevated N_2O emission. In urban rivers and lakes, biological saturation¹⁷, characterized by nonlinear relationships such as efficiency loss models²⁶ and exponential models²⁷, has been observed due to excessive nutrient input. Therefore, it is imperative to re-evaluate the relationship between N_2O emissions and nutrient concentration, as well as the applicability of the current EF_{5e} in human-influenced estuaries.

To address these knowledge gaps, we carried out a high-resolution measurement campaign for N_2O concentrations and fluxes in the Pearl River Estuary (PRE), China—a typical wastewater-influenced estuary. We quantify the impact of wastewater discharge on estuarine N_2O emissions and identify the likely biochemical processes that shape N_2O dynamics and their spatial heterogeneity in the PRE. Through a meta-analysis, we further examine the distinct patterns of N_2O emission in response to nitrogen input from wastewater in global estuaries. Despite their relatively small surface area, wastewater-influenced estuaries emit disproportionately high levels of N_2O . Meanwhile, due to the progressive biological saturation of N_2O production, where the

supply of available nitrate exceeds biological demand, the EF_{5e} in wastewater-influenced estuaries is significantly lower than in undisturbed estuaries and the current IPCC's global level. The findings of this study demonstrate the important role that wastewater nitrogen discharges play in shaping estuarine N_2O emissions, highlighting the need to revise the emission factor and consequently the regional and global N_2O inventories.

Results and discussion

Heterogeneous N_2O concentrations and high emission fluxes in the PRE region. Our high-resolution monitoring campaign, consisting of ~30,000 real-time N_2O concentration measurements (Fig. 1a and Supplementary Data in the figshare repository: <https://doi.org/10.6084/m9.figshare.24129774>), reveals substantial spatial variations in dissolved N_2O concentrations across the PRE region. Concentrations ranged from 9.1 to 132.2 nmol L^{-1} with an average of $31.7 \pm 26.5 \text{ nmol L}^{-1}$ (Fig. 2a). The vast majority of PRE exhibited N_2O supersaturation (140.91–1723.07%) (Fig. 2b), suggesting that the estuary is a net source of atmospheric N_2O ²⁸. N_2O concentrations, in general, follow an inland-to-sea gradient, with higher mean concentrations observed upstream of Humen (zone i) at $69.9 \pm 27.7 \text{ nmol L}^{-1}$, decreasing to $13.1 \pm 2.3 \text{ nmol L}^{-1}$ downstream of the estuary (zone iii) (Fig. 2a). Concentration ranges in zones i, ii, and iii were 30.5–132.2 nmol L^{-1} , 13.0–86.4 nmol L^{-1} , and 9.1–20.7 nmol L^{-1} , respectively, while the corresponding saturation ranges were 415–1723%, 177–1119%, and 141–284%. Along the west-to-east transect, slightly higher N_2O concentrations were observed on the west side (12.8 nmol L^{-1}) compared with the east side (9.1 nmol L^{-1}) (transect III). Our high-resolution monitoring also provides detailed insights into the spatial heterogeneity of N_2O concentrations. Notably, we observed a hotspot of N_2O concentration to the northwest of Inner Lingding island (Fig. 2a), where N_2O concentrations reached $25.5 \pm 3.9 \text{ nmol L}^{-1}$, significantly higher than the surrounding areas (p -value < 0.001).

Similarly, water–air N_2O flux exhibited substantial spatial variability in the PRE, varying by up to two orders of magnitude (5.5–308.3 $\mu\text{mol m}^{-2} \text{ d}^{-1}$). The average N_2O flux was $58.5 \pm 65.7 \mu\text{mol m}^{-2} \text{ d}^{-1}$ (Fig. 2c), which is three times the global estuarine average (18.2 $\mu\text{mol m}^{-2} \text{ d}^{-1}$; range: 2.4–199.2 $\mu\text{mol m}^{-2} \text{ d}^{-1}$)³. The average flux density in the PRE was comparable to that reported in other human-impacted estuaries, such as Schelde (66.6 $\mu\text{mol m}^{-2} \text{ d}^{-1}$)²⁹, Thames (69.1 $\mu\text{mol m}^{-2} \text{ d}^{-1}$)³⁰, and Humber (76.6 $\mu\text{mol m}^{-2} \text{ d}^{-1}$)³¹ estuaries in Europe, Werribee estuary (78 $\mu\text{mol m}^{-2} \text{ d}^{-1}$)³² in Oceania, and Tokay estuary (77.3 $\mu\text{mol m}^{-2} \text{ d}^{-1}$)³³ and Adyar estuary (44.3 $\mu\text{mol m}^{-2} \text{ d}^{-1}$)³⁴ in Asia.

Our high-resolution monitoring enables reliable estimation of N_2O emissions. As suggested by previous observations in the PRE, there are no strong seasonal variations in N_2O concentrations/emissions within the middle and lower estuaries¹⁷. In comparison, the upstream of Humen exhibits clear seasonal patterns: N_2O concentrations and fluxes in winter and spring are 0.75–2.5 times (on average 1.5 times) higher than in summer and fall^{17,24}. Considering this seasonal variability in the upstream of Humen, we estimate an annual emission of 1.05×10^9 (9.22×10^8 – 1.23×10^9) g N_2O from the entire PRE to the atmosphere. This emission level is comparable to the total emissions from 19 European inner estuaries³¹, which cover an area of approximately 1840 km^2 and emit 1.35×10^9 g $\text{N}_2\text{O yr}^{-1}$. Given that the median annual global N_2O flux³ is 0.23 (range: 0.13–0.44) Tg, the PRE contributes 4.6% of global estuarine N_2O emissions while covering only 1.4% of global estuarine areas. Especially, despite comprising only ~8% of the PRE's surface area, the upstream section (zone i) accounts for up to 42.16% of

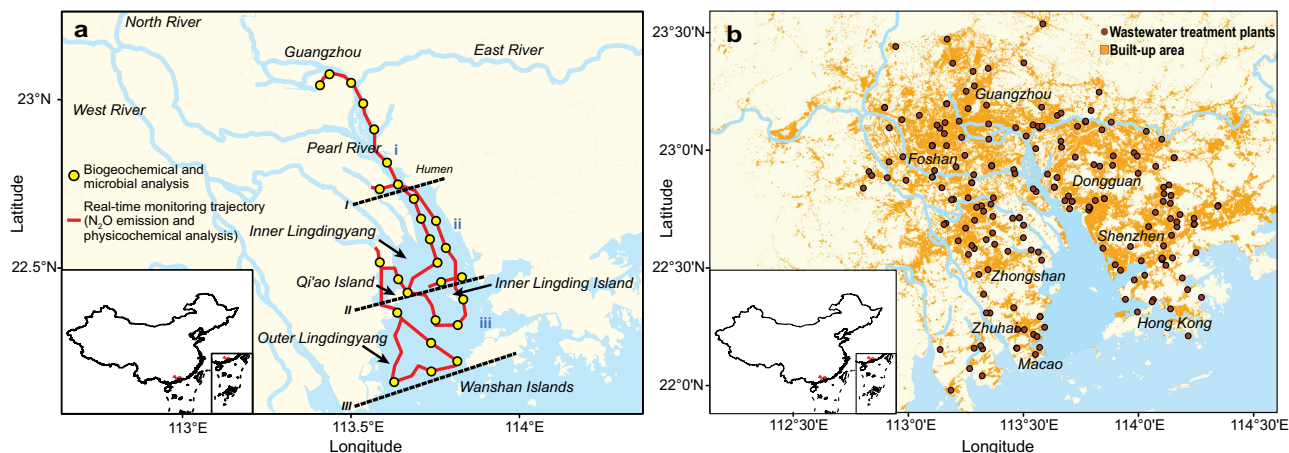


Fig. 1 Real-time high-resolution monitoring trajectory in the PRE and surrounding wastewater treatment plants. **a** Monitoring trajectory and sampling sites. Along the monitoring trajectory (red curve), ~30,000 data points of N_2O concentrations and environmental parameters (Chlorophyll a, dissolved oxygen (DO), oxidation reduction potential (ORP), salinity, conductivity, total dissolved solids (TDS), turbidity, pH, and temperature) were collected. Yellow circles indicate sampling sites where biogeochemical parameters ($\text{NH}_4\text{-N}$, $\text{NO}_2\text{-N}$, $\text{NO}_3\text{-N}$, dissolved inorganic nitrogen (DIN), dissolved organic carbon (DOC), and total phosphorus (TP)) as well as ammonia-oxidizing and denitrifying microbial genes with qPCR (*AOA amoA*, *AOB amoA*, *nirS*, *nirK*, *nosZ*, and *narG*) were analyzed. The entire PRE is divided into three zones: (1) Upstream of Humen (upper estuary; zone i); (2) Inner Lingdingyang (middle estuary; zone ii between I and II); (3) Outer Lingdingyang (lower estuary; zone iii between II and III). **b** Distribution of wastewater treatment plants and built-up areas around the PRE. Wastewater treatment plants shown in (b) are national key monitoring wastewater treatment plants in Guangzhou, Shenzhen, Dongguan, Foshan, Zhongshan, Zhuhai, and major wastewater treatment plants in Hong Kong and Macao. The inset shows the study area in red on the map of China. The base map is from RESDC data (<http://www.resdc.cn/>).

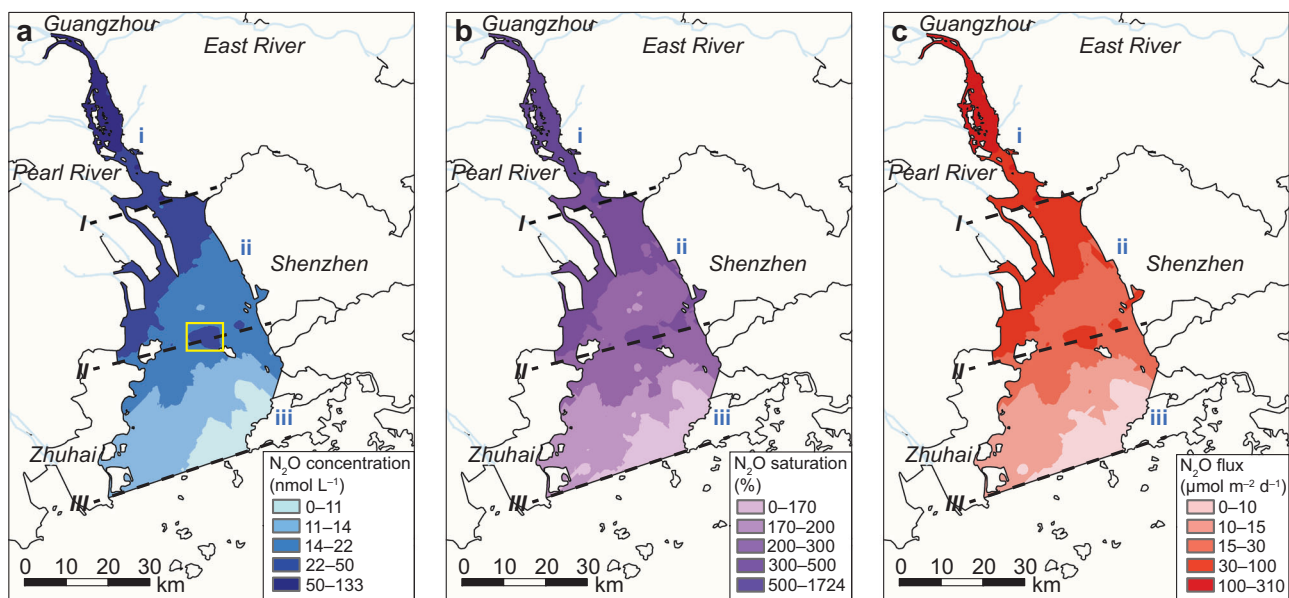


Fig. 2 Spatial distribution of N_2O concentrations, saturations, and air-water fluxes in the PRE. **a** Dissolved N_2O concentrations. **b** N_2O saturations. **c** N_2O fluxes. Spatial distributions were interpolated from high-resolution, real-time data (Supplementary Fig. 3) using Kriging interpolation. The yellow box in (a) indicates the N_2O concentration hotspot to the northwest of Inner Lingding Island. The base map is from RESDC data (<http://www.resdc.cn/>).

N_2O emissions. When expressed in terms of 100-year global warming potential (GWP), N_2O emissions ($6.3 \times 10^9 \text{ mol yr}^{-1} \text{ CO}_2\text{-equivalent}$) are equivalent to ~21% of CO_2 emissions ($3 \times 10^{10} \text{ mol yr}^{-1} \text{ CO}_2$)³⁵ or 161% of CH_4 emission ($3.92 \times 10^9 \text{ mol yr}^{-1} \text{ CO}_2\text{-equivalent}$)³⁶ from the PRE. This amount is also close to ~9.3% of the CO_2 sink in the coastal systems of the entire China³⁷.

Impacts of wastewater discharges on N_2O emissions in the PRE region. Increasing urban wastewater load can greatly enhance estuarine N_2O production^{5,21}. Surrounded by numerous wastewater treatment plants (Fig. 1b), the PRE received 5.55×10^8

tons of treated wastewater in 2021³⁸. When further accounting for indirect discharges from surrounding cities, this figure could reach up to 6.80×10^9 tons³⁹. Assuming a dissolved inorganic nitrogen (DIN) concentration in wastewater effluent of 15 mg L^{-1} , which follows the highest discharge standard (Class 1A) for total nitrogen (TN) in municipal wastewater treatment plants in China (GB18918-2002), DIN input is estimated to be $(5.95\text{--}72.90) \times 10^8 \text{ mol}$. Considering the relatively consistent wastewater discharges over time, we estimate a DIN load of $(0.16\text{--}2.00) \times 10^7 \text{ mol d}^{-1}$ for both dry and wet seasons.

In addition to wastewater discharges, nutrient inputs from submarine groundwater and upstream river sources are also

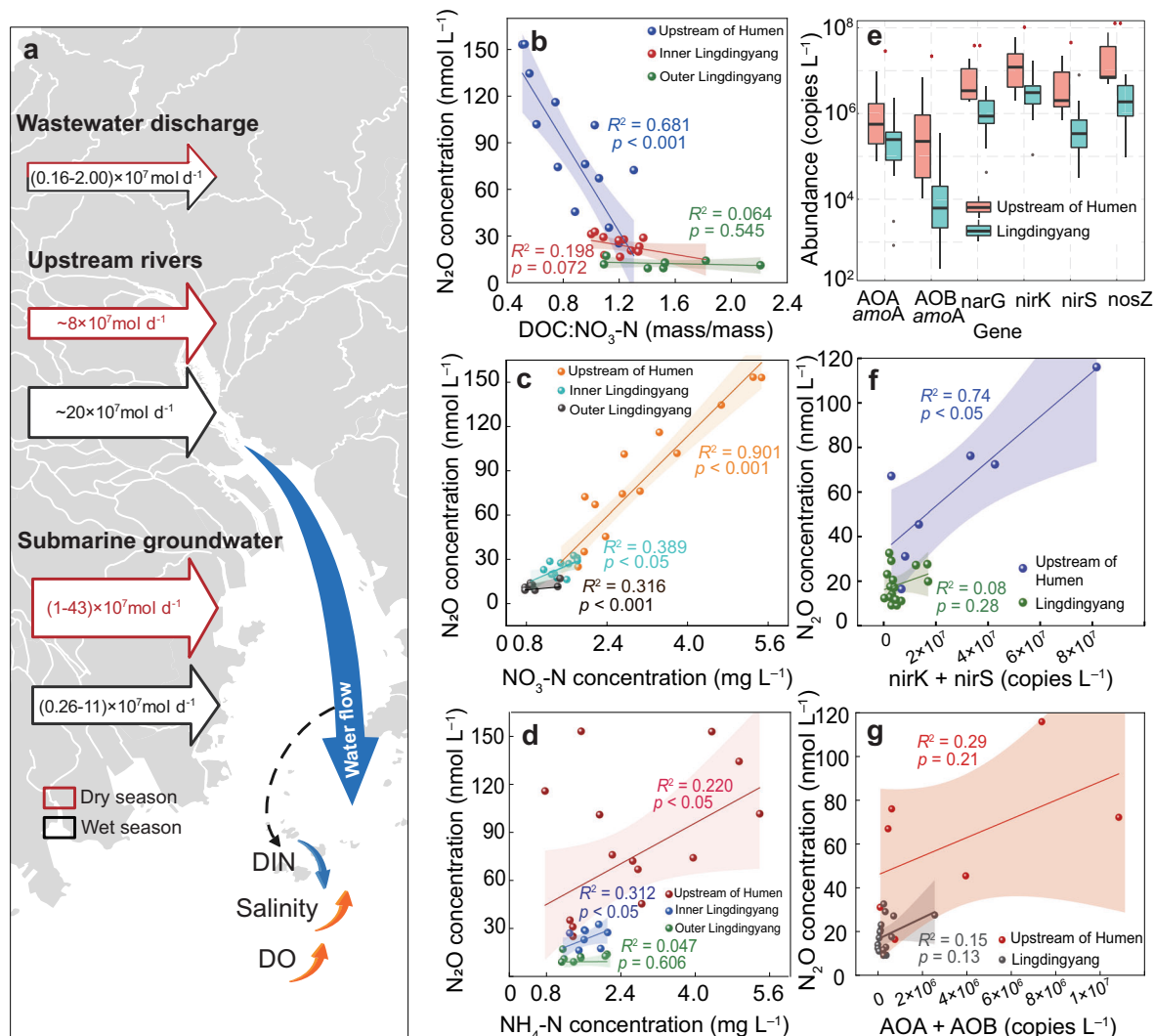


Fig. 3 Influence of wastewater discharges and drivers of N_2O emissions in the PRE. **a** N input from wastewater discharge, submarine groundwater, and upstream rivers, and spatial variations of key physicochemical parameters DIN, salinity, and DO. Upward/downward arrow denotes increasing/decreasing trend from upstream to downstream. Detailed spatial distributions of all physicochemical parameters are in Supplementary Fig. 5. **b** Relationship between N_2O concentration and DOC:NO₃-N concentration. **c** Relationship between dissolved N_2O concentration and NO₃-N concentration. **d** Relationship between dissolved N_2O concentration and NH₄-N concentration. **e** Abundances and significance of spatial differences in ammonia-oxidizing and denitrification genes in the PRE. Symbols “****”, “***”, and “**” denote different significance levels with p -values <0.001, 0.01 and 0.05, respectively. **f** Linear regression between N_2O concentrations and abundances of denitrifying genes (*nirS* and *nirK*). **g** Linear regression between N_2O concentrations and abundances of ammonia-oxidizing genes (AOA and AOB *amoA*). Shaded areas in (b, c, d, f, and g) show the 95% confidence bands.

important. By applying the ²²⁴Ra mass balance model, submarine groundwater discharges in the PRE are estimated to contribute water flows of $(4.5-10) \times 10^8 \text{ m}^3 \text{ d}^{-1}$ and $(1.2-2.7) \times 10^8 \text{ m}^3 \text{ d}^{-1}$ in the dry season and wet season, respectively⁴⁰. These flows result in DIN loads of $(1.0-43) \times 10^7 \text{ mol d}^{-1}$ and $(0.26-11) \times 10^7 \text{ mol d}^{-1}$ during the respective seasons⁴⁰. For riverine nutrient input, the estimated values of DIN loads are $\sim 8 \times 10^7 \text{ mol d}^{-1}$ during the dry season and $\sim 20 \times 10^7 \text{ mol d}^{-1}$ during the wet season⁴⁰. The contribution of nutrient input from wastewater discharges is comparable to that from submarine groundwater and upstream rivers, suggesting its vital role in regulating the nutrient budget and stoichiometry in the PRE (Fig. 3a). Additionally, the relative high TN to total phosphorus (TP) ratios observed in the aquatic system are associated with submarine groundwater discharge⁴⁰ and rapid improvements in wastewater treatment⁴¹, which can potentially contribute to N_2O emissions in the estuary⁴².

The upper section of the PRE exhibited higher concentrations of DOC and DIN (Supplementary Fig. 4), primarily influenced by the influx of carbon and nitrogen from nearby urban wastewater treatment plants. With 97 centralized wastewater treatment plants in Guangzhou and Dongguan surrounding the area, the upstream of Humen received 175,081 thousand tons of treated wastewater in 2021, resulting in a discharge intensity per unit area more than four times higher than that in the middle and lower sections³⁸. The increasing DIN loads can lead to the formation of hypoxic and anoxia zones in estuaries⁴³. In the upstream section of the PRE, lower dissolved oxygen concentrations were observed (Supplementary Fig. 5), which can further stimulate denitrification and result in a high $N_2O:N_2$ ratio under high NO₃-N concentration conditions¹⁹ (Supplementary Fig. 4).

Compared with natural estuaries, the discharge from wastewater treatment plants in human-influenced estuaries exhibits lower carbon-to-nitrogen ratios, potentially leading to different

N_2O production rates and yields. N_2O concentrations upstream of Humen (zone i) showed a negative correlation with the ratio of DOC to $\text{NO}_3\text{-N}$ ($R^2 = 0.681$, p -value < 0.001) (Fig. 3b). This correlation suggests a possible link between N_2O emission and the nitrogen reduction process¹⁷. With limited DOC relative to $\text{NO}_3\text{-N}$, denitrification slows down or halts at N_2O or NO_2^- instead of fully converting to N_2 . It is noteworthy that the average ratio of DOC to $\text{NO}_3\text{-N}$ upstream of PRE was significantly lower compared to five other subtropical estuaries in China²¹, where denitrification is favored during N_2O production. In addition, dissolved N_2O showed a relatively stronger correlation with $\text{NO}_3\text{-N}$ concentration ($R^2 = 0.901$, p -value < 0.001) than with $\text{NH}_4\text{-N}$ concentration ($R^2 = 0.220$, p -value < 0.05) in the upstream of Human (Fig. 3c, d), indicating a higher contribution of denitrification and DNRA to N_2O production compared with nitrification and nitrifier denitrification¹⁴.

The presence of abundant ammonia-oxidizing and denitrifying genes in the PRE (Fig. 3e) indicates that N_2O production is collectively mediated by nitrifying and denitrifying microorganisms. In general, the total abundance of denitrifying genes (*nirK*, *nirS*, *narG*, and *nosZ*) was much higher than that of AOA *amoA* and AOB *amoA*, with the upstream section of Humen showing higher gene abundances than the middle and lower sections (Fig. 3e). N_2O concentrations showed a positive correlation with the abundance of denitrifying bacterial *nirS* and *nirK* genes in the upstream section ($R^2 = 0.74$, p -value < 0.05) (Fig. 3f), suggesting the important role of denitrification in upstream N_2O production²¹. In comparison, N_2O concentrations exhibited a stronger correlation with the abundance of ammonia-oxidizing genes than with that of denitrifying genes in Lingdingyang (Fig. 3g). The contribution of nitrification in the upper and middle sections is also supported by the positive correlations between N_2O concentration and $\text{NH}_4\text{-N}$ substrate (Fig. 3d), aligning with observations in other anthropogenically influenced estuaries²¹.

Overall, the combined effects of abundant nutrient input, low C:N ratios, and relatively low dissolved oxygen levels induced by wastewater discharges collectively stimulate N_2O emissions. Stronger denitrification occurs in the upstream section of the PRE, which intensifies the spatial heterogeneity of N_2O distribution and complicates the biogeochemical processes associated with N_2O emissions.

Disproportionately high N_2O emissions from global wastewater-influenced estuaries. To better understand the impact of wastewater discharges on estuarine N_2O emissions, we investigate the nitrogen input from wastewater⁴⁴ and associated N_2O emissions in 83 estuaries worldwide through a meta-analysis (Fig. 4 and Supplementary Data in the figshare repository: <https://doi.org/10.6084/m9.figshare.24129774>). On a global scale, dissolved N_2O concentrations were positively correlated with wastewater nitrogen input ($R^2 = 0.15$, p -value < 0.05) (Fig. 5a), suggesting a higher contribution of exogenous nitrogen to N_2O emissions in wastewater-influenced estuaries. Based on the levels of nitrogen from wastewater discharges, we classify global estuaries into two groups. Compared with estuaries experiencing lighter wastewater influence (nitrogen $< 2 \text{ Mg N km}^{-2}$), highly wastewater-influenced estuaries (nitrogen $\geq 2 \text{ Mg N km}^{-2}$) exhibited significantly higher N_2O flux (p -value < 0.001 , t -test) (Fig. 5c), with a median emission level of $32.20 \mu\text{mol m}^{-2} \text{ d}^{-1}$ (95% CI: $13.30\text{--}48.10 \mu\text{mol m}^{-2} \text{ d}^{-1}$).

Estuaries facing increasing anthropogenic stress are playing an increasingly important role in predicting future global N_2O emissions and assessing climate feedback. Globally, approximately 52% of the total nitrogen load in estuarine and riverine

watersheds originates from anthropogenic sources¹³, aligning closely with the estimate of 56% (based on the ratio of anthropogenic to total nitrogen additions from land) used in calculating anthropogenic estuarine emissions in global N_2O budget¹⁴. Enhanced nitrogen load resulted in an additional $2.6\text{--}9.9 \text{ Gmol yr}^{-1}$ of $\text{N}_2\text{O-N}$ emission from estuaries and rivers¹³. Meanwhile, estimates of estuarine N_2O emissions are associated with large uncertainties due to the interaction of human influences with biochemical processes, leading to limited constraints on both marine and global N_2O budgets. Notably, global N_2O emissions were estimated to be $\sim 17.0 \text{ Tg N yr}^{-1}$ ¹⁴, with $\sim 4.2 \text{ Tg N yr}^{-1}$ originating from the ocean⁴⁵. Therefore, enhancing the accuracy of estuarine N_2O emission estimates is crucial to better constrain its contribution to marine and global budgets, especially under anthropogenic perturbations.

N_2O emission factors in wastewater-influenced estuaries are significantly lower than the current IPCC EF_{5e} . We further calculate N_2O emission factors (EF_{5e}) for PRE and 82 other estuaries globally. Across all estuaries, N_2O emission factor is negatively correlated with nitrogen input from wastewater discharge ($R^2 = 0.34$, p -value < 0.05) (Fig. 5b), suggesting a reduced contribution of nitrogen input to water-to-air N_2O diffusive emissions in response to increases nutrient substrate. The N_2O emission factor for PRE is $0.00052 \pm 0.00022 \text{ kg N}_2\text{O-N/kg NO}_3\text{-N}$, while the median EF_{5e} for highly wastewater-influenced estuaries globally is 0.00078 (95% CI: $0.00034\text{--}0.00116$) $\text{kg N}_2\text{O-N/kg NO}_3\text{-N}$. Both values are significantly lower than the IPCC's default value of $0.0026 \text{ kg N}_2\text{O-N/kg NO}_3\text{-N}$ ²⁰. Even the median EF_{5e} for estuaries with low wastewater influences globally— 0.00138 (95% CI: 0.00086 to 0.00181) $\text{kg N}_2\text{O-N/kg NO}_3\text{-N}$ —is lower than the IPCC level. The discrepancy suggests that the current global estuarine N_2O emission factor used by IPCC is overestimated by up to an order of magnitude, particularly in estuaries with high wastewater influences.

Previous studies have also revealed large uncertainties associated with the IPCC's EF_{5e} estimate^{13,21}. Mechanistic modeling approaches that kinetically limit the extent of biochemical reactions have been used to estimate the ranges of emission factors for estuaries¹³. The results consistently indicate that IPCC's emission factors are too high to be universally applied across all estuaries. For example, Kroeze et al. applied the IPCC default emission factor to estimate global estuarine N_2O emissions at 100 Gg N yr^{-1} with a TN input of 44 Tg yr^{-1} ⁴⁶. However, if we consider the latest TN load estimate of 97.6 Tg yr^{-1} ¹³, estuarine N_2O emissions would be approximately 220 Gg N yr^{-1} when using the IPCC's default emission factor, significantly higher than the estimate of $60\text{--}155 \text{ Gg N yr}^{-1}$ from that based on kinetically mechanistic modeling^{13,14}.

We analyze the relationship between the observed N_2O and $\text{NO}_3\text{-N}$ concentrations (Supplementary Table 1) using three models that incorporate biochemical reaction kinetics in N_2O production (Fig. 6). The linear model assumes a 1st-order response, in which N_2O concentrations are directly proportional to $\text{NO}_3\text{-N}$ concentrations⁴⁷. The efficiency loss model describes a power relationship with an exponent (or order) less than one, indicating that N_2O production by the biota increases with $\text{NO}_3\text{-N}$ availability, but the efficiency of N_2O concentrations relative to $\text{NO}_3\text{-N}$ concentrations declines²⁶. The third model employs Michaelis–Menten uptake kinetics, representing a saturation of N_2O production as the supply of available $\text{NO}_3\text{-N}$ exceeds biological demand⁴⁸.

Globally, the functional relationship between biological N_2O production and $\text{NO}_3\text{-N}$ concentration is best described by the efficiency loss model ($R^2 = 0.49$, p -value < 0.05) (Fig. 6a), in

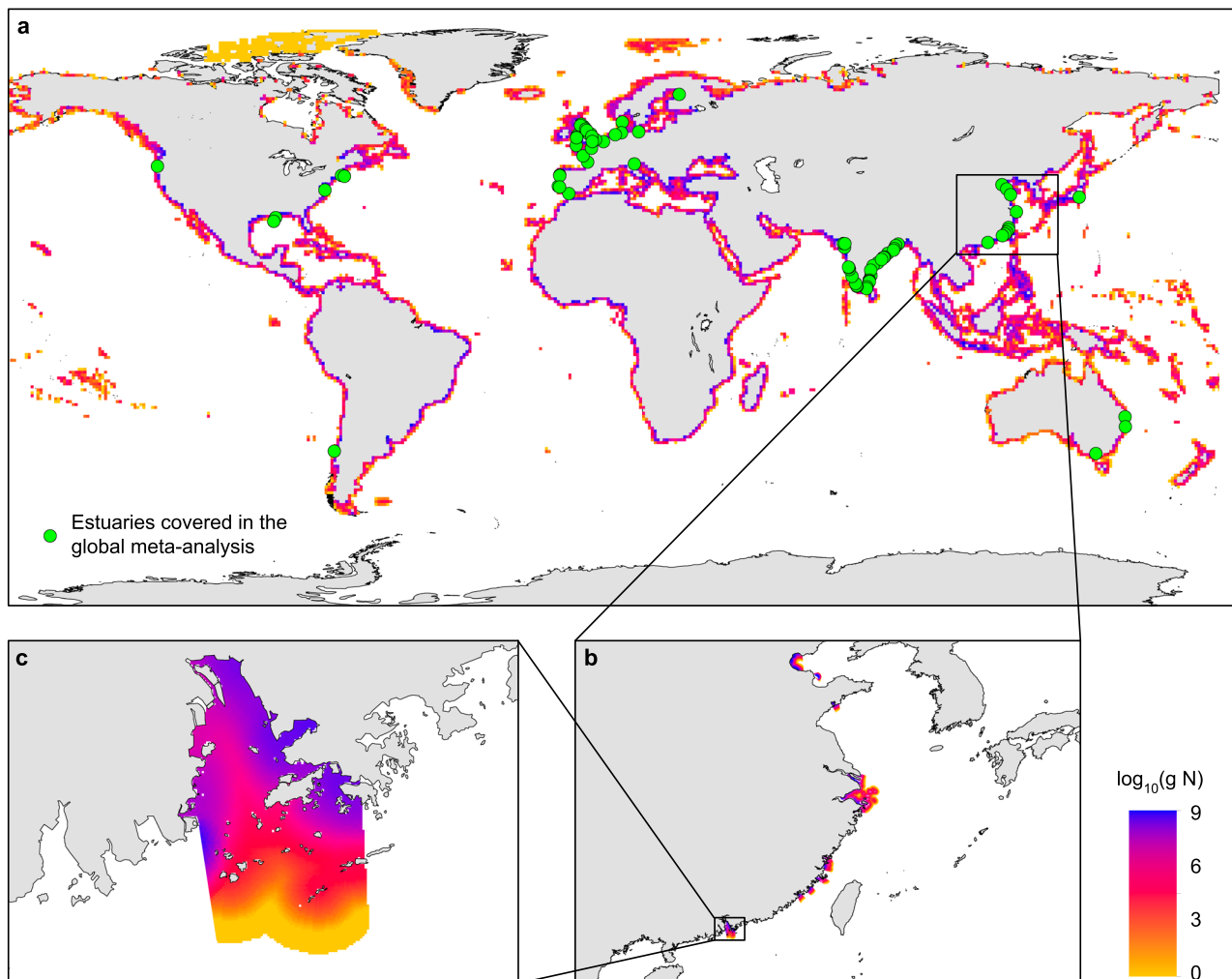


Fig. 4 Wastewater nitrogen in global estuaries. **a** Distribution of wastewater nitrogen input in global estuaries. **b** Zoomed-in view of estuarine wastewater nitrogen in China. **c** Zoomed-in view of estuarine wastewater nitrogen in the PRE. Wastewater nitrogen input is shown in $\log_{10}(\text{g N})$. Green circles in **(a)** represent the 83 estuaries covered in the meta-analysis. Zoomed-in view of different continents are shown in Supplementary Fig. 6.

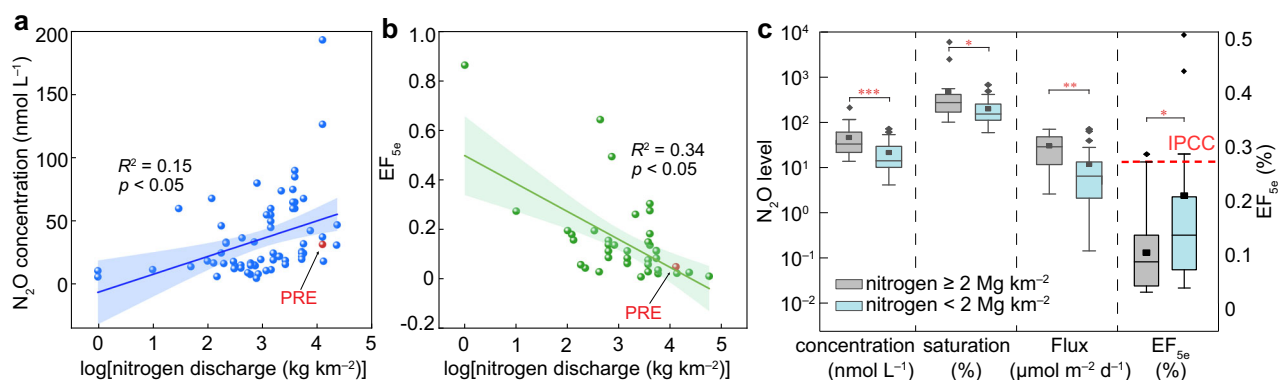


Fig. 5 N_2O emissions influenced by wastewater nitrogen discharge in global estuaries. **a** N_2O concentration in relation to wastewater nitrogen discharge, **b** EF_{5e} in relation to wastewater nitrogen discharge. **c** Levels of N_2O concentration, saturation, emission flux, and emission factors (EF_{5e}) in two groups of estuaries worldwide with different levels of wastewater nitrogen discharge (estuaries with high human impacts: wastewater nitrogen $\geq 2 \text{ Mg N km}^{-2}$; estuaries with low human impacts: wastewater nitrogen $< 2 \text{ Mg N km}^{-2}$). Details of estuaries are summarized in Supplementary Data in the figshare repository: <https://doi.org/10.6084/m9.figshare.24129774>. Symbols “****”, “***”, and “**” in **(c)** denote p -values < 0.001 , 0.01 , and 0.05 , respectively. Shaded areas in **(a)** and **(b)** show the 95% confidence bands.

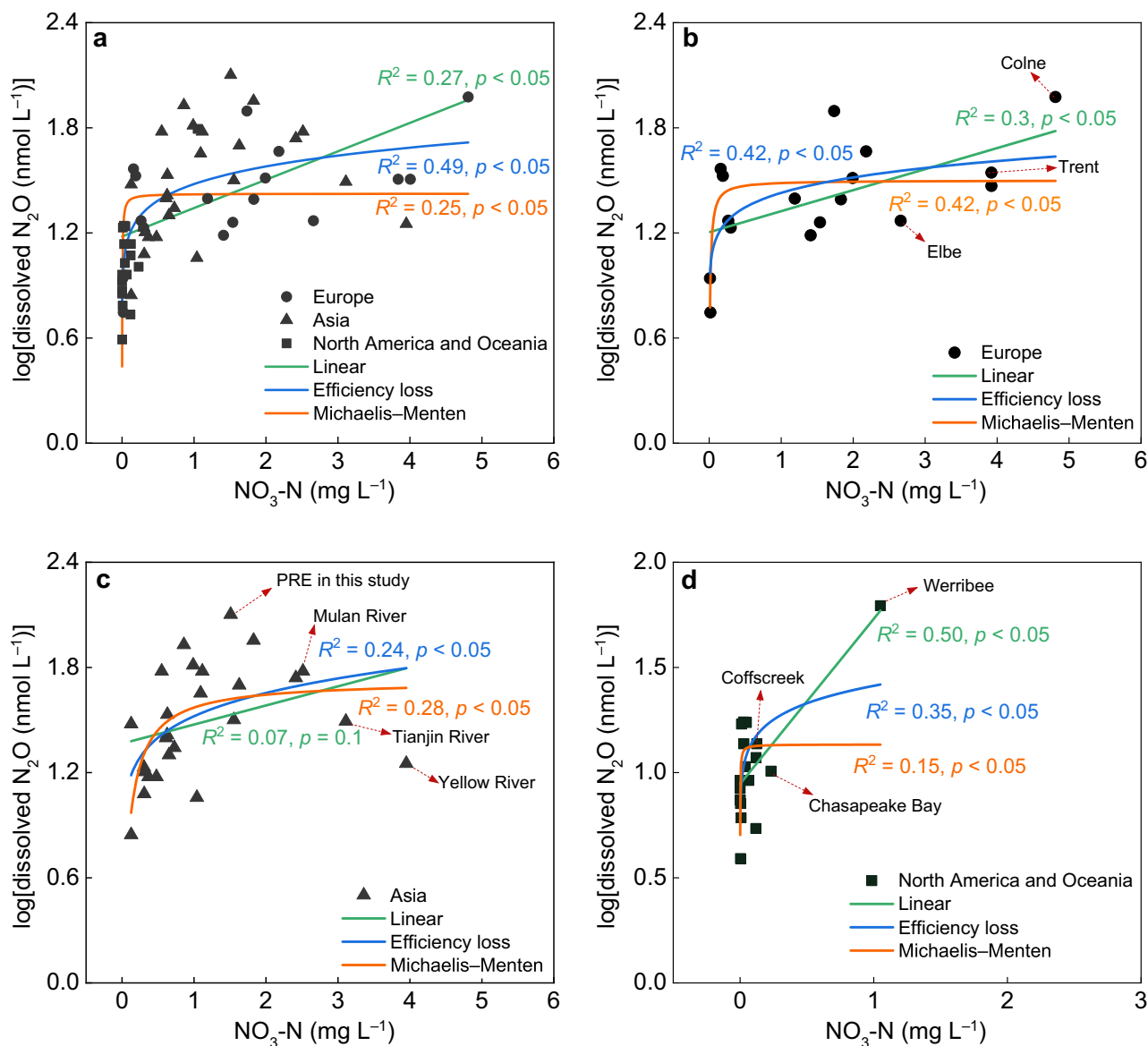


Fig. 6 Relationships between N_2O concentrations and $\text{NO}_3\text{-N}$ concentrations characterized by linear model, efficiency loss model, and Michaelis-Menten kinetics models in estuaries worldwide. a Global estuaries. **b** European estuaries. **c** Asian estuaries. **d** North American and Oceanian estuaries. Goodness-of-fit statistics including residual sum of squares (RSE), adjusted R^2 , root mean square error (RMSE), and Akaike information criterion (AIC) are summarized in Supplementary Table 1.

which the efficiency of N_2O production decreases with increasing $\text{NO}_3\text{-N}$ availability. This efficiency loss model is particularly evident in microbial communities adapted to chronic loading, showing high flexibility in response to increasing nutrient concentrations and thus a delayed saturation⁴⁹. In European and Asian estuaries (Fig. 6b, c), better performance is observed for the Michaelis-Menten model with $R^2 = 0.42$ and 0.28 , respectively. These results show that N_2O production initially increases linearly with $\text{NO}_3\text{-N}$ concentration but then plateaus at around 1600 nmol L^{-1} when $\text{NO}_3\text{-N}$ concentration exceeds $\sim 3 \text{ mg L}^{-1}$, similar to observations in wastewater-influenced inland water¹⁷. This plateau is mainly attributed to progressive biological saturation in processing nitrogen with increasing DIN load^{50,51}. While the number of favorable denitrification and nitrification sites at the water-sediment interface remains relatively constant⁵², the efficiency of denitrification and

nitrification decreases with increasing nitrogen inputs, eventually leading to relatively stable N_2O emissions at high $\text{NO}_3\text{-N}$ levels.

Estuaries with high levels of dissolved N_2O saturation are widespread along the coasts of West Europe, Southern Asia, and Eastern Asia, including estuaries such as Colne and Trent estuaries in the UK (Fig. 6b) and the Yellow River and Tianjin River estuaries in China (Fig. 6c). It is noteworthy that data for European estuaries are primarily from the 1980s and 2000s. In comparison, for Asian estuaries, especially in rapidly developing countries such as China and India, the projected increase in nutrient load³ is expected to maintain high N_2O emissions. In North America and Oceania (Fig. 6d), a linear model is a better fit for the response of N_2O to $\text{NO}_3\text{-N}$, indicating that the increase in nitrogen input can linearly translate to elevated N_2O emissions under conditions of low substrate concentration. This pattern is consistent with observations in estuaries such as Werribee

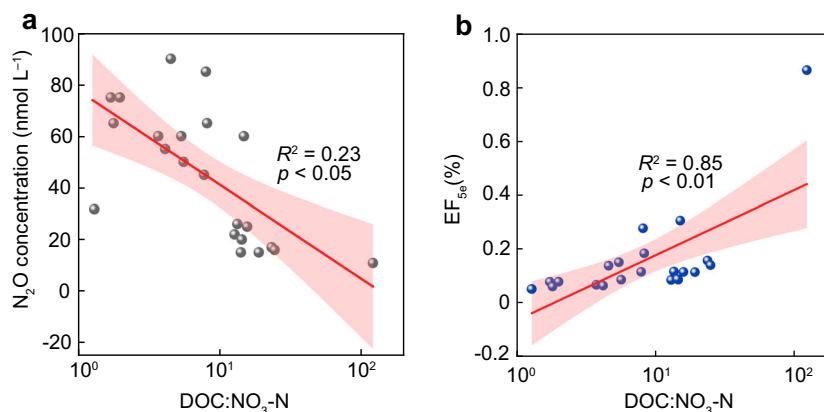


Fig. 7 Dissolved N_2O concentration and emission factor as functions of $\text{DOC}:\text{NO}_3\text{-N}$ in global estuaries. **a** Relationship between dissolved N_2O concentration and $\text{DOC}:\text{NO}_3\text{-N}$. **b** Relationship between EF_{5e} and $\text{DOC}:\text{NO}_3\text{-N}$. Red lines are linear regression fits, with shaded areas showing the 95% confidence bands.

Estuary in Australia and Chesapeake Bay in the USA. Additional fitness statistics for the three models in different estuaries are summarized in Supplementary Table 1.

Refining the IPCC estimate to constrain global estuarine N_2O emission contribution. The assumption of a linear response of N_2O -N to $\text{NO}_3\text{-N}$ by IPCC is not always valid, as demonstrated by the results discussed earlier. Therefore, it is crucial to develop a global mechanistic model that explicitly captures the spatial and dynamic relationship between substrate availability and N_2O emissions. Such a model would provide a more accurate representation of the complex processes occurring in estuaries.

A mechanistic modeling approach for predicting N_2O emissions was developed previously¹³, which incorporates water residence time as a key factor. This refinement adds an important kinetic dimension to existing N_2O estimates and better constrains the extent of denitrification and nitrification processes. Additionally, considering piecewise EF_{5e} under different nitrogen load conditions could be an alternative approach to improving the estimation of estuarine N_2O emissions. Previous studies have also shown the potential of using regression models based on bottom-up data to derive global riverine N_2O emission factors across continents and climate zones⁵². Despite these advancements in models, the combination of monitoring efforts and modeling endeavors remains essential for improving the accuracy of estuarine N_2O emission estimates.

Specifically, it is crucial to reconsider the role of denitrification and its contribution to N_2O emissions in human-influenced estuaries. The assumption made by the IPCC that nitrification produces twice as much N_2O as denitrification^{53,54} has been a subject of controversy. Recent studies have reported global nitrification and denitrification fluxes in estuaries to be approximately $0.69 \text{ Tmol yr}^{-1}$ and $0.66 \text{ Tmol yr}^{-1}$, respectively¹³, indicating a higher contribution from denitrification than suggested by the IPCC. Observations in various estuaries, such as Humber³³, Clone^{55,56}, Tianjin⁵⁷, Mulan river²¹, and Pear River estuaries, have demonstrated intense N_2O production associated with denitrification, particularly under high $\text{NO}_3\text{-N}$ concentrations as shown in Fig. 6.

In the presence of high DIN loads and low oxygen conditions, denitrification can be stimulated¹⁸, and N_2O is not efficiently consumed as an electron acceptor, resulting in a high $\text{N}_2\text{O}:\text{N}_2$ ratio (higher than 5%) in estuaries influenced by urban wastewater¹⁹. This phenomenon is common in eutrophic waters and the upper reaches of estuaries³. In comparison, in organic-rich environments, denitrification potential is limited by nitrate

availability¹⁹. In the case of the PRE, influenced by wastewater discharges, the ratios of $\text{DOC}:\text{DIN}$ and $\text{DOC}:\text{NO}_3\text{-N}$ are 0.51 ± 0.09 and 1.25 ± 0.29 , respectively, much lower than the levels found in global rivers (average $\text{DOC}:\text{NO}_3\text{-N}$: 55)⁵⁸ and agriculture/forestlands (median $\text{DOC}:\text{DIN}$: 10)⁵². Globally, there is a negative correlation between estuarine $\text{DOC}:\text{NO}_3\text{-N}$ and N_2O concentration ($R^2 = 0.23$, p -value < 0.05) (Fig. 7a) but a positive correlation with EF_{5e} ($R^2 = 0.85$, p -value < 0.01) (Fig. 7b). Therefore, in addition to nutrient, organics and C:N stoichiometry should be considered as important variables for estimating N_2O emissions, especially in denitrification-dominant estuaries.

Taken together, the abundant nutrient loads and altered substrate stoichiometry ratio in highly wastewater-influenced estuaries, such as PRE, favor N_2O production through nitrification and especially denitrification processes. Consequently, these estuaries often exhibit disproportionately high N_2O emissions, which contribute positively to global warming. However, as the nitrogen load continues to increase, the dissolved N_2O concentration gradually reaches a plateau due to progressive biological saturation. The systematic overestimation of estuarine N_2O emission based on the IPCC's emission factor mentioned above results from the assumption that N_2O emission linearly responds to nitrogen input. Therefore, it is crucial to refine the relationship between N_2O emission and DIN substrate and subsequently revise EF_{5e} and global estuarine N_2O emission estimates. This can potentially be achieved through appropriate modeling of the kinetic relationship between carbon and nitrogen substrates with estuarine N_2O emissions. Additionally, the current study underscores the significance of comprehensive bottom-up monitoring efforts, as they are essential and indispensable for validating and improving the accuracy of models.

Methods

Study area. The Pearl River Estuary (PRE) is located between Guangzhou ($23^\circ 10' \text{ N}$) and the Wanshan Islands ($22^\circ 00' \text{ N}$), covering an area of $\sim 1794.6 \text{ km}^2$, where Pearl River, the second largest river in China in terms of annual water discharge ($3.3 \times 10^{11} \text{ m}^3 \text{ yr}^{-1}$), flows into the South China Sea. Surrounded by metropolitan areas such as Hong Kong, Shenzhen, and Guangzhou, this subtropical estuary bears substantial influence from human activities. There are in total of 436 centralized wastewater treatment plants, including 199 national key monitoring plants (Fig. 1b) densely distributed throughout the PRE^{38,59,60}. The designed capacity of these plants is $23,813 \times 10^3 \text{ m}^3 \text{ d}^{-1}$, of which $4942 \times 10^3 \text{ m}^3 \text{ d}^{-1}$ is directly discharged into the estuary³⁸. In 2021, the PRE received $554,897 \times 10^3$ tons of treated wastewater

discharge³⁸, a figure that could potentially soar to $6,803,960 \times 10^3$ tons when further accounting for additional indirect discharges from surrounding cities³⁹. Human activities, especially wastewater discharge, have led to hypoxia⁶¹ and eutrophication²⁸ within the PRE, promoting elevated N₂O emissions. Given the ongoing urbanization and industrialization trends, N₂O emissions from the PRE are expected to further increase in the near future.

We carried out field measurements from October 28 to November 1, 2021, continuously monitoring dissolved N₂O concentrations in the water column during a 5-day cruise. To better understand spatial variations in N₂O emissions, we divided the entire study area into three zones based on both N₂O concentrations and the geometry of the estuary. Zone i, upstream of Humen (upper estuary), spans from tidal channels in Guangzhou to the Humen Outlet, covering an area of ~143 km². Zone ii, Inner Lingdingyang (middle estuary), extends from the Humen Outlet to Inner Lingding Island, encompassing an area of ~848 km². Zone iii, Outer Lingdingyang (lower estuary), stretches from Inner Lingding Island to the Outer Estuary, covering an area of ~804 km².

N₂O concentration measurements. We conducted continuous N₂O concentration measurements using a fast-response automated gas equilibrator⁶² attached to a gas analyzer (N₂O M1-916; LGR, Canada) aboard a ship during the 5-day field campaign, covering the entire PRE (Fig. 1a). The measured N₂O mole fraction was then converted to dissolved concentration in the water column using a device-specific calibration curve, accounting for both partial equilibrations within the device⁶² and temperature-dependent solubility⁶³. We obtained in total 28,351 individual measurements of dissolved N₂O concentrations, with the sampling locations recorded via GPS. We subsequently interpolated the spatial distribution across the entire PRE using Kriging.

We also measured multiple physicochemical parameters, including Chlorophyll a, dissolved oxygen (DO), oxidation reduction potential (ORP), salinity, conductivity, total dissolved solids (TDS), turbidity, pH, and temperature using a multi-parameter probe (EXO2, YSI, USA) (see Supplementary Data in the figshare repository: <https://doi.org/10.6084/m9.figshare.24129774>). In addition, we collected surface water samples at representative sites for biogeochemical and microbial analyses (yellow circles in Fig. 1a). Air temperature, air pressure, and wind speed were measured in situ with a portable anemometer (YGY-QXY). Annual air temperature and precipitation data were obtained from the National Meteorological Information Center (<http://data.cma.cn/>).

Fast-Response Automated Gas Equilibrator (FaRAGE) system.

Continuous measurement of N₂O concentration was based on the Fast-Response Automated Gas Equilibrator (FaRAGE) system⁶² coupled with a greenhouse gas analyzer (Supplementary Fig. 1). The FaRAGE system is a low-cost equilibrator designed to achieve rapid gas–water equilibration, making it well-suited for field campaigns. The FaRAGE operates as a flow-through system, introducing gas flow into a constant water flow to create a minimal headspace for continuous concentration measurements. It comprises two main components: a gas–water mixing unit and a gas–water separation unit. In the gas–water mixing unit, water is continuously pumped into a 50-mL chamber using a peristaltic pump at a rate of 250 mL min⁻¹. They are then thoroughly mixed with the carrier gas. Efficient degassing is achieved through the jet flow entering the chamber and the generation of micro-bubbles in the water tube and bubble diffusor and is further enhanced in a

2-m long coiled tube (Tygon; inner diameter: 4 mm). The gas–water separation unit then separates headspace gas from water through gravity, after which the headspace gas is directed to the greenhouse gas analyzer for measurement. Our tests suggested that the response time of the FaRAGE system (including the response time of the gas analyzer) was 41 ± 2 s (Supplementary Fig. 2). Note that the measured concentration in the headspace was adjusted by considering the background N₂O concentration in the carrier gas (N₂, 99.9%). The FaRAGE system has been calibrated⁶² and applied to high-frequency, real-time monitoring of N₂O and CH₄ concentrations in the Three Gorges Reservoir^{64,65} and CH₄ emissions in the upper reaches of the Mekong River⁶⁶, which has enabled accurate high-resolution mapping of gas concentration distributions.

Flux calculation. The N₂O flux across the water–air interface can be estimated using the following equation

$$F = k \times (C_0 - C_e) \quad (1)$$

where F ($\mu\text{mol m}^{-2} \text{d}^{-1}$) is the flux, k (cm h^{-1}) is the normalized gas transfer velocity depending on wind and water temperatures, C_0 is the N₂O concentration measured in the water, and C_e is the N₂O concentration in equilibrium with the atmospheric concentration.

The N₂O equilibrium concentration is calculated based on Henry's law as⁶³

$$C_e = x' K_0 (P - p\text{H}_2\text{O}) \exp \left[P \left(\frac{B + 2\delta}{RT} + \bar{v} \left(\frac{1 - P}{RT} \right) \right) \right] \quad (2)$$

$$\ln p\text{H}_2\text{O} = 24.4543 - 67.4509 \left(\frac{100}{T} \right) - 4.8489 \ln \left(\frac{T}{100} \right) - 0.000544S \quad (3)$$

where x' is the mole fraction of a constituent of dry air (the global abundance of N₂O was 333.2 ± 0.1 ppb in 2020 according to the Global Atmosphere Watch Programme's in situ observation network; <http://www.wmo.int>), K_0 is the equilibrium constant ($\text{mol L}^{-1} \text{atm}^{-1}$), P is the total pressure, $p\text{H}_2\text{O}$ is the vapor pressure of water (atm), as a polynomial function of temperature (T) and salinity (S) in Eq. (3), \bar{v} is the partial molal volume, R is the gas constant ($0.08205601 \text{ L atm mol}^{-1} \text{K}^{-1}$), and the term $\frac{B+2\delta}{RT}$ is calculated as

$$\frac{B + 2\delta}{RT} = -\frac{9.4563}{T} + 0.04739 - 6.427 \times 10^{-5}T \quad (4)$$

The gas transfer velocity (k) of N₂O is calculated as⁶⁷

$$k = 0.251 \times u_{10}^2 \left(Sc / Sc_{(20^\circ\text{C})} \right)^{-0.5} \quad (5)$$

where Sc is the Schmidt number, and the value for 20 °C is 600 and 660 in freshwater and seawater, respectively; u_{10} is the 10-m wind speed and derived from wind speed measurements conducted at a height of 4 m⁶⁸. The temperature-dependent Schmidt number Sc for N₂O in freshwater (Sc_f) and seawater (Sc_s) is calculated respectively using⁶⁷

$$Sc_f = 2141.2 - 152.56T + 5.8963T^2 - 0.12411T^3 + 0.0010655T^4 \quad (6)$$

$$Sc_s = 2356.2 - 166.38T + 6.3952T^2 - 0.13422T^3 + 0.0011506T^4 \quad (7)$$

Freshwater condition is used for the upstream of Humen (upper estuary; zone i), and seawater condition is used for Lingdingyang (middle and lower estuary; zones ii and iii).

Biogeochemical analyses. Collected water samples were filtered on-site through 0.45 μm polyethersulfone (PES) syringe filters to measure concentrations of $\text{NO}_3\text{-N}$, $\text{NO}_2\text{-N}$, $\text{NH}_4\text{-N}$, and DOC. The filtrates were collected in 500 ml plastic sampling bottles, and the pH was adjusted to below 2 by adding H_2SO_4 . Concentrations of $\text{NO}_3\text{-N}$, $\text{NO}_2\text{-N}$, and $\text{NH}_4\text{-N}$ were then measured by UV spectrophotometry, naphthylamine hydrochloride spectrophotometry, and hypobromite oxidation methods, respectively. DOC concentrations were determined using a TOC analyzer (Shimadzu TOC-5000, Japan) through high-temperature catalytic oxidation. TP concentrations were measured using an ultraviolet-visible spectrophotometer (Agilent 1200) with the standard molybdenum blue method after persulphate digestion.

Microbial analysis. A total of 27 surface water samples were collected and filtered through 0.22 μm PES filters, and these samples were prepared in triplicate for microbial analysis. DNA from particle-associated and free-living bacterial communities was extracted from approximately 1.5 L homogenized surface water (filtered with membrane) using an E.Z.N.A. soil DNA Kit (Omega Bio-tek, Norcross, GA, USA). The DNA extracts were checked using 1% agarose gel. Subsequently, DNA concentration and purity were determined using a NanoDrop 2000 ultraviolet-visible spectrophotometer (Thermo Scientific, Wilmington, USA). After DNA extraction, real-time quantitative polymerase chain reaction (qPCR) was employed to estimate the abundances of ammonia-oxidizing (AOA and AOB *amoA*) and denitrifying bacterial genes (*nirK*, *nirS*, *narG*, and *nosZ*). The abundances of ammonia monooxygenase (AOA and AOB *amoA*) genes were amplified using primer pair sets arch-*amoA*-23F/arch-*amoA*-616R and CTO189f/CTO654r. For denitrifying gene abundances, we used primer sets cd3aF/R3cd, FlaCu/R3cu, nosZF/nosZR, and narG-f/narG-r, which encompass the known diversity of dissimilatory nitrite reductase (*nirS* and *nirK*), nitrous oxide reductase (*nosZ*), and nitrate reductase (*narG*). qPCR assays were performed in triplicate on an ABI7300 Thermal Cycler (Applied Biosystems, USA). Further details on qPCR primer pairs and amplification conditions can be found in Supplementary Table 2. A 10-fold dilution series was obtained from extracted plasmid DNA with a known copy number and was used to generate an external standard curve. The amplification efficiencies of the archaeal *amoA*, bacterial *amoA*, *nirS*, *nirK*, *narG*, and *nosZ* genes ranged from 89 to 104%, with all amplifications achieving R^2 values greater than 0.99.

Global estuarine meta-analysis. To examine the impact of anthropogenic stress on estuarine N_2O emission flux and associated spatial patterns, we conducted a meta-analysis on nitrogen input from wastewater⁴⁴ and N_2O emissions in estuaries worldwide. Our dataset includes estuarine emission data from Asia, Europe, North America, South America and Oceania, spanning from the 1980s to the present. We synthesized information on variable parameters such as dissolved N_2O concentration, N_2O flux, saturation, EF_{5e} , $\text{NO}_3\text{-N}$, and $\text{DOC}:\text{NO}_3\text{-N}$ (Supplementary Data in the figshare repository: <https://doi.org/10.6084/m9.figshare.24129774>). To determine coastal nitrogen distribution resulting from wastewater input, we used a high-resolution (~ 1 km) global dataset⁴⁴, which considers sewerage, septic, and untreated wastewater inputs in 142,625 watersheds or coastal areas. The propagation of nitrogen effluent from each pourpoint into coastal waters was quantified using a plume model based on a logarithmic decay function⁶⁹. We extracted wastewater nitrogen input data for individual estuaries using ArcGIS 10.4. The delineation of estuarine boundaries, represented as irregular polygons, was cross-verified against other studies. For each estuary,

we calculated grid-level statistics, including maximum, mean, and standard deviation, for wastewater nitrogen input using Python 3.7. The distribution of wastewater nitrogen in 83 estuaries worldwide is shown in Fig. 4 and Supplementary Fig. 6, with detailed statistics summarized in Supplementary Data in the figshare repository: <https://doi.org/10.6084/m9.figshare.24129774>.

Generating global estimates from a limited pool of data inevitably introduces uncertainties. These uncertainties primarily stem from the highly uneven spatial distribution of the available in situ measurements, which have been predominantly concentrated in industrialized regions of Asia, Europe, and North America, with limited research efforts in Africa and South America. Nevertheless, our study includes a substantial number of wastewater-influenced estuaries, enhancing our understanding of N_2O dynamics in these environments.

For global estuarine data analysis, we performed linear regression and *t*-test in R. Prior to linear regression analysis, we identified and removed outliers based on box plots. Additionally, we assessed the statistical significance of differences in N_2O concentrations, N_2O fluxes, N_2O saturations, and EF_{5e} values using *t*-test.

Fitting linear, efficiency loss, and Michaelis-Menten kinetics models. We applied the linear model, efficiency loss model, and Michaelis-Menten kinetics model to evaluate the relationship between dissolved N_2O concentration and nitrate concentration. To create a comprehensive global overview, we compiled estuarine data from both previous studies and the present study (Supplementary Data in the figshare repository: <https://doi.org/10.6084/m9.figshare.24129774>).

Linear regression⁴⁷ was used to fit the 1st-order response of N_2O concentrations to $\text{NO}_3\text{-N}$ concentrations:

$$C = k \times [\text{NO}_3^-] \quad (8)$$

where C represents the N_2O concentration.

In the efficiency loss model²⁶, the N_2O production by biota increases with rising $\text{NO}_3\text{-N}$ concentrations, while the efficiency of N_2O production relative to $\text{NO}_3\text{-N}$ concentrations declines. This model employs a power relationship in which the exponent is less than one ($n < 1$):

$$C = k \times [\text{NO}_3^-]^n \quad (9)$$

The Michaelis-Menten kinetics⁴⁸ model depicts the N_2O production as the supply of $\text{NO}_3\text{-N}$ exceeds biological demand:

$$C = \frac{C_{\max} \times [\text{NO}_3^-]}{K_m + [\text{NO}_3^-]} \quad (10)$$

where C_{\max} represents the maximum N_2O concentration achieved in the estuaries, and K_m is the required $\text{NO}_3\text{-N}$ concentration to achieve half of C_{\max} .

Throughout these regression analyses, we applied a log transformation to the dependent variables to reduce the leverage effects of high N_2O concentrations. The assessment of model fit, including the residual sum of squares (RSE), adjusted R^2 , root mean square error (RMSE), and Akaike information criterion (AIC) are summarized in Supplementary Table 1.

Reporting summary. Further information on research design is available in the Nature Portfolio Reporting Summary linked to this article.

Data availability

Data collected and compiled in this study are available in the figshare repository: <https://doi.org/10.6084/m9.figshare.24129774>.

Received: 25 February 2023; Accepted: 11 October 2023;

Published online: 27 October 2023

References

- Ravishankara, A. R., Daniel, J. S. & Portman, R. W. Nitrous oxide (N₂O): the dominant ozone-depleting substance emitted in the 21st century. *Science* **326**, 120–123 (2009).
- Xu, P. et al. Policy-enabled stabilization of nitrous oxide emissions from livestock production in China over 1978–2017. *Nat. Food* **3**, 356–366 (2022).
- Murray, R. H., Erler, D. V. & Eyre, B. D. Nitrous oxide fluxes in estuarine environments: response to global change. *Glob. Chang. Biol.* **21**, 3219–3245 (2015).
- Bange, H. W., Rapsomanik, S. & Andreae, M. O. Nitrous oxide in coastal waters. *Glob. Biogeochem. Cycles* **10**, 197–207 (1996).
- Brown, A. M., Bass, A. M. & Pickard, A. E. Anthropogenic-estuarine interactions cause disproportionate greenhouse gas production: a review of the evidence base. *Mar. Pollut. Bull.* **174**, 113240 (2022).
- Harley, J. F. et al. Spatial and seasonal fluxes of the greenhouse gases N₂O, CO₂ and CH₄ in a UK macrotidal estuary. *Estuar. Coast. Shelf Sci.* **153**, 62–73 (2015).
- Quick, A. M. et al. Nitrous oxide from streams and rivers: a review of primary biogeochemical pathways and environmental variables. *Earth Sci. Rev.* **191**, 224–262 (2019).
- Murray, R., Erler, D., Rosentreter, J., Maher, D. & Eyre, B. A seasonal source and sink of nitrous oxide in mangroves: insights from concentration, isotope, and isotopomer measurements. *Geochim. Cosmochim. Acta* **238**, 169–192 (2018).
- Xia, X., Jia, Z., Liu, T., Zhang, S. & Zhang, L. Coupled nitrification-denitrification caused by suspended sediment (SPS) in rivers: importance of SPS size and composition. *Environ. Sci. Technol.* **51**, 212–221 (2017).
- Ni, J. et al. Three Gorges Dam: friend or foe of riverine greenhouse gases? *Natl Sci. Rev.* **9**, nwa013 (2022).
- Rosentreter, J. A. et al. Coastal vegetation and estuaries are collectively a greenhouse gas sink. *Nat. Clim. Change* **13**, 579–587 (2023).
- Galloway, J. N. et al. The nitrogen cascade. *Bioscience* **53**, 341–356 (2003).
- Maavara, T. et al. Nitrous oxide emissions from inland waters: are IPCC estimates too high? *Glob. Chang. Biol.* **25**, 473–488 (2019).
- Tian, H. et al. A comprehensive quantification of global nitrous oxide sources and sinks. *Nature* **586**, 248–256 (2020).
- Wang, D. et al. Treatment of municipal sewage with low carbon-to-nitrogen ratio via simultaneous partial nitrification, anaerobic ammonia oxidation, and denitrification (SNAD) in a non-woven rotating biological contactor. *Chemosphere* **208**, 854–861 (2018).
- Deng, S., Li, D., Yang, X., Zhu, S. & Li, J. Process of nitrogen transformation and microbial community structure in the Fe(0)–carbon-based bio-carrier filled in biological aerated filter. *Environ. Sci. Pollut. Res.* **23**, 6621–6630 (2016).
- Xia, X. et al. Distinctive patterns and controls of nitrous oxide concentrations and fluxes from urban inland waters. *Environ. Sci. Technol.* **55**, 8422–8431 (2021).
- Chen, G. C., Tam, N. F. Y., Wong, Y. S. & Ye, Y. Effect of wastewater discharge on greenhouse gas fluxes from mangrove soils. *Atmos. Environ.* **45**, 1110–1115 (2011).
- Teixeira, C., Magalhães, C., Boaventura, R. A. R. & Bordalo, A. A. Potential rates and environmental controls of denitrification and nitrous oxide production in a temperate urbanized estuary. *Mar. Environ. Res.* **70**, 336–342 (2010).
- IPCC. *Chapter 11: N₂O Emissions from Managed Soils, and CO₂ Emissions from Lime and Urea Application*. IPCC Guidelines for National Greenhouse Gas Inventories (IPCC, 2019).
- Li, X. et al. Nitrous oxide emissions from subtropical estuaries: insights for environmental controls and implications. *Water Res.* **212**, 118110 (2022).
- Yu, Z. et al. Nitrous oxide emissions in the Shanghai river network: implications for the effects of urban sewage and IPCC methodology. *Glob. Chang. Biol.* **19**, 2999–3010 (2013).
- Song, K. et al. Distinctive microbial processes and controlling factors related to indirect N₂O emission from agricultural and urban rivers in Taihu watershed. *Environ. Sci. Technol.* **56**, 4642–4654 (2022).
- Dong, Y., Xu, L., Yang, Z., Zheng, H. & Chen, L. Aggravation of reactive nitrogen flow driven by human production and consumption in Guangzhou City China. *Nat. Commun.* **11**, 1209 (2020).
- Yang, P. et al. Large variations in indirect N₂O emission factors (EF₅) from coastal aquaculture systems in China from plot to regional scales. *Water Res.* **200**, 117208 (2021).
- O'Brien, J. M., Dodds, W. K., Wilson, K. C., Murdock, J. N. & Eichmiller, J. The saturation of N cycling in Central Plains streams: 15N experiments across a broad gradient of nitrate concentrations. *Biogeochemistry* **84**, 31–49 (2007).
- Zhou, Y. et al. Nonlinear pattern and algal dual-impact in N₂O emission with increasing trophic levels in shallow lakes. *Water Res.* **203**, 117489 (2021).
- Lin, H. et al. Spatiotemporal variability of nitrous oxide in a large eutrophic estuarine system: the Pearl River Estuary, China. *Mar. Chem.* **182**, 14–24 (2016).
- De Wilde, H. P. J. & De Bie, M. J. M. Nitrous oxide in the Schelde estuary: production by nitrification and emission to the atmosphere. *Mar. Chem.* **69**, 203–216 (2000).
- De Bie, M. J. M., Middelburg, J. J., Starink, M. & Laanbroek, H. J. Factors controlling nitrous oxide at the microbial community and estuarine scale. *Mar. Ecol. Prog. Ser.* **240**, 1–9 (2002).
- Barnes, J. & Upstill-Goddard, R. C. N₂O seasonal distributions and air-sea exchange in UK estuaries: implications for the tropospheric N₂O source from European coastal waters. *J. Geophys. Res. Biogeosci.* **116**, G01006 (2011).
- Wong, W. W. et al. Dynamics of groundwater-derived nitrate and nitrous oxide in a tidal estuary from radon mass balance modeling. *Limnol. Oceanogr.* **58**, 1689–1706 (2013).
- Hashimoto, S., Gojo, K., Hikota, S., Sendai, N. & Otsuki, A. Nitrous oxide emissions from coastal waters in Tokyo Bay. *Mar. Environ. Res.* **47**, 213–223 (1999).
- Nirmal Rajkumar, A., Barnes, J., Ramesh, R., Purvaja, R. & Upstill-Goddard, R. C. Methane and nitrous oxide fluxes in the polluted Adyar River and estuary, SE India. *Mar. Pollut. Bull.* **56**, 2043–2051 (2008).
- Guo, X., Dai, M., Zhai, W., Cai, W.-J. & Chen, B. CO₂ flux and seasonal variability in a large subtropical estuarine system, the Pearl River Estuary, China. *J. Geophys. Res.* **104**, G03013 (2009).
- Ye, W., Zhang, G., Zheng, W., Zhang, H. & Wu, Y. Methane distributions and sea-to-air fluxes in the Pearl River Estuary and the northern South China Sea. *Deep-Sea Res. Part II Top. Stud. Oceanogr.* **167**, 34–45 (2019).
- Yi, S. L. *Measuring the Value of Blue Carbon in China Coastal Zone* (In Chinese with English Abstract). Master's thesis, Xiamen University (2017).
- Department of Ecology and Environment of Guangdong Province. Monitoring information of direct discharge from marine pollution sources in Guangdong province. <http://gdee.gd.gov.cn/> (2022).
- Ministry of Housing and Urban-Rural Construction of the People's Republic of China. *China Urban Construction Statistical Yearbook* (China Statistics Press, 2022).
- Liu, J., Du, J., Wu, Y. & Liu, S. Nutrient input through submarine groundwater discharge in two major Chinese estuaries: the Pearl River Estuary and the Changjiang River Estuary. *Estuar. Coast. Shelf Sci.* **203**, 17–28 (2018).
- Tong, Y. et al. Improvement in municipal wastewater treatment alters lake nitrogen to phosphorus ratios in populated regions. *Proc. Natl Acad. Sci. USA* **117**, 11566–11572 (2020).
- Wells, N. S. et al. Estuaries as sources and sinks of N₂O across a land use gradient in subtropical Australia. *Glob. Biogeochem. Cycles* **32**, 877–894 (2018).
- Howarth, R. et al. Coupled biogeochemical cycles: eutrophication and hypoxia in temperate estuaries and coastal marine ecosystems. *Front. Ecol. Environ.* **9**, 18–26 (2011).
- Tuholske, C. et al. Mapping global inputs and impacts from human sewage in coastal ecosystems. *PLoS ONE* **16**, e0258898 (2021).
- Yang, S. et al. Global reconstruction reduces the uncertainty of oceanic nitrous oxide emissions and reveals a vigorous seasonal cycle. *Proc. Natl Acad. Sci. USA* **117**, 11954–11960 (2020).
- Kroeze, C., Dumont, E. & Seitzinger, S. Future trends in emissions of N₂O from rivers and estuaries. *J. Integr. Environ. Sci.* **7**, 71–78 (2010).
- Dodds, W. K. et al. N uptake as a function of concentration in streams. *J. North Am. Benthol. Soc.* **21**, 206–220 (2002).
- Turner, P. A. et al. Regional-scale controls on dissolved nitrous oxide in the Upper Mississippi River. *Geophys. Res. Lett.* **43**, 4400–4407 (2016).
- Pucher, M. et al. Complex interactions of in-stream dissolved organic matter and nutrient spiralling unravelled by Bayesian regression analysis. *Biogeosciences* **18**, 3103–3122 (2021).
- Mulholland, P. J. et al. Stream denitrification across biomes and its response to anthropogenic nitrate loading. *Nature* **452**, 202–205 (2008).
- Peterson, B. J. et al. Control of nitrogen export from watersheds by headwater streams. *Science* **292**, 86–90 (2001).
- Hu, M., Chen, D. & Dahlgren, R. A. Modeling nitrous oxide emission from rivers: a global assessment. *Glob. Chang. Biol.* **22**, 3566–3582 (2016).
- Beaulieu, J. J. et al. Nitrous oxide emission from denitrification in stream and river networks. *Proc. Natl Acad. Sci. USA* **108**, 214–219 (2011).
- Mosier, A. et al. Closing the global N₂O budget: nitrous oxide emissions through the agricultural nitrogen cycle. *Nutr. Cycl. Agroecosyst.* **52**, 225–248 (1998).

55. Robinson, A. D., Nedwell, D. B., Harrison, R. M. & Ogilvie, B. G. Hypernutriented estuaries as sources of N₂O emission to the atmosphere: the estuary of the River Colne, Essex, UK. *Mar. Ecol. Prog. Ser.* **164**, 59–71 (1998).
56. Dong, L. F., Nedwell, D. B., Underwood, G. J. C., Thornton, D. C. O. & Rusmana, I. Nitrous oxide formation in the Colne estuary, England: the central role of nitrite. *Appl. Environ. Microbiol.* **68**, 1240–1249 (2002).
57. Liu, X. L. et al. Nitrous oxide emissions from river network with variable nitrogen loading in Tianjin, China. *J. Geochem. Explor.* **157**, 153–161 (2015).
58. Stanley, E. H. et al. The ecology of methane in streams and rivers: patterns, controls, and global significance. *Ecol. Monogr.* **86**, 146–171 (2016).
59. Drainage Services Department of Hong Kong. Sewage treatment plants in Hong Kong. <https://www.dsd.gov.hk/> (2023).
60. Environmental Protection Agency of Macao. Sewage treatment plants in Macao. <https://www.dspa.gov.mo/> (2023).
61. Qian, W. et al. Current status of emerging hypoxia in a eutrophic estuary: the lower reach of the Pearl River Estuary, China. *Estuar. Coast. Shelf Sci.* **205**, 58–67 (2018).
62. Xiao, S., Liu, L., Wang, W., Lorke, A. & Woodhouse, J. A Fast-Response Automated Gas Equilibrator (FaRAGE) for continuous in situ measurement of CH₄ and CO₂ dissolved in water. *Hydrol. Earth Syst. Sci.* **24**, 3871–3880 (2020).
63. Weiss, R. F. & Price, B. A. Nitrous oxide solubility in water and seawater. *Mar. Chem.* **8**, 347–359 (1980).
64. Guo, X. et al. Density currents reduce nitrous oxide emissions in a tributary bay of Three Gorges Reservoir. *Water Res.* **190**, 116750 (2021).
65. Liu, J. et al. Spatial and temporal variability of dissolved methane concentrations and diffusive emissions in the Three Gorges Reservoir. *Water Res.* **207**, 117788 (2021).
66. Liu, L. et al. Spatial and temporal variability of methane emissions from cascading reservoirs in the Upper Mekong River. *Water Res.* **186**, 116319 (2020).
67. Wanninkhof, R. Relationship between wind speed and gas exchange over the ocean revisited. *Limnol. Oceanogr. Methods* **12**, 351–362 (2014).
68. Amorcho, J. & DeVries, J. J. A new evaluation of the wind stress coefficient over water surfaces. *J. Geophys. Res.* **85**, 433 (1980).
69. Halpern, B. S. et al. A global map of human impact on marine ecosystems. *Science* **15**, 948–952 (2008).

Acknowledgements

This research was supported by the National Natural Science Foundation of China (No. 52100208 and 51979148), Guangdong Basic and Applied Basic Research Fund (2020A1515110098), and Guangdong-Hong Kong Joint Laboratory for Water Security (2020B1212030005). We gratefully acknowledge Xingyu Yuan, Yu Ma, Ying Guo, Zhilong Zhao, Yuqi Huang, and Hongying Wang for their assistance with the biochemical analysis of water samples, and Xiangwang Zheng, Jieming Hu, Xingyu Yuan, Yu Ma, Shuai Liu, and Zhanliang Zhu for their support in the fieldwork.

Author contributions

Y.D., S.W., S.X., and C.W. designed the study. Y.D. and C.W. wrote the first draft of the manuscript. Y.D., J.L., X.C., W.L., and C.Z. carried out the fieldwork. Y.D., J.L., X.C., F.F., W.L., C.Z., and C.L. performed lab analysis and data procurement. Y.D., X.C., Y.L., and C.L. conducted model simulations. Y.D., X.C., C.L., and C.W. prepared figures. All authors contributed to the interpretation and the preparation of the final manuscript.

Competing interests

The authors declare no competing interests.

Additional information

Supplementary information The online version contains supplementary material available at <https://doi.org/10.1038/s43247-023-01051-6>.

Correspondence and requests for materials should be addressed to Shengrui Wang, Shangbin Xiao or Chenghao Wang.

Peer review information *Communications Earth & Environment* thanks Damian Arevalo-Martinez and the other anonymous reviewer(s) for their contribution to the peer review of this work. Primary handling editors: Annie Bourbonnais, Clare Davis. A peer review file is available.

Reprints and permission information is available at <http://www.nature.com/reprints>

Publisher's note Springer Nature remains neutral with regard to jurisdictional claims in published maps and institutional affiliations.



Open Access This article is licensed under a Creative Commons Attribution 4.0 International License, which permits use, sharing, adaptation, distribution and reproduction in any medium or format, as long as you give appropriate credit to the original author(s) and the source, provide a link to the Creative Commons licence, and indicate if changes were made. The images or other third party material in this article are included in the article's Creative Commons licence, unless indicated otherwise in a credit line to the material. If material is not included in the article's Creative Commons licence and your intended use is not permitted by statutory regulation or exceeds the permitted use, you will need to obtain permission directly from the copyright holder. To view a copy of this licence, visit <http://creativecommons.org/licenses/by/4.0/>.

© The Author(s) 2023